ChemPubSoc Europe

DOI: 10.1002/chem.201904541

CHEMISTRY A European Journal Full Paper

Ultrafast Spectroscopy

# A Unified Experimental/Theoretical Description of the Ultrafast Photophysics of Single and Double Thionated Uracils

Danielle Cristina Teles-Ferreira[+],[a, b] Irene Conti[+],[c] Rocío Borrego-Varillas[+],[d] Artur Nenov[+],[c] Ivo H. M. Van Stokkum,[e] Lucia Ganzer,[d] Cristian Manzoni,[d] Ana Maria de Paula,*[a] Giulio Cerullo,*[d] and Marco Garavelli*[c]

**Abstract:** Photoinduced processes in thiouracil derivatives have lately attracted considerable attention due to their suitability for innovative biological and pharmacological applications. Here, sub-20 fs broadband transient absorption spectroscopy in the near-UV are combined with CASPT2/MM decay path calculations to unravel the excited-state decay channels of water solvated 2-thio and 2,4-dithiouracil. These molecules feature linear absorption spectra with overlapping ππ* bands, leading to parallel decay routes which we systematically track for the first time. The results reveal that different processes lead to the triplet states population, both directly from the ππ* absorbing state and via the intermediate nπ* dark state. Moreover, the 2,4-dithiouracil decay pathways is shown to be strongly correlated either to those of 2- or 4-thiouracil, depending on the sulfur atom on which the electronic transition localizes.

## Introduction

Thiobases are nucleobase derivatives obtained by the replacement of oxygen atoms in the canonical exocyclic carbonyl group with sulfur.[1,2] Thionation redshifts the absorption spectra[3] and radically changes the photophysics[4] of sulfur-substituted bases. In nucleobases, after UV-light absorption, ultrafast nonradiative repopulation of the ground state occurs through conical intersections (CIs),[5] leading to their remarkable photostability.[6] In contrast, in thiobases the main photoexcited state deactivation pathway is intersystem crossing (ISC) to long-lived reactive triplet states. The selective UV absorption and the high triplet quantum yield[7–9] confer to thiobases great potential in the field of photodynamic therapeutic applications[10–14] as well as for their use as photolabels.[15–17] Elucidating the photophysical mechanisms leading to population of the triplet state and their timescales has become increasingly relevant.[8,9,18–20] To date, transient absorption (TA) spectroscopy experiments, with approximately 200-fs time resolution, for 2-thiouracil (2TU), 4-thiouracil (4TU) and 2,4-dithiouracil (24TU) have shown an ultrafast ISC occurring within hundreds of femtoseconds.[7,10,21] For 2TU[21–27] and 4TU,[28,29] high-level calculations have pointed out two possible energy relaxation pathways from the lowest bright excited singlet state: direct ISC to the triplet manifold or a two-step process, whereby the population of the triplet state is mediated by a dark singlet state of nπ* symmetry.[18,20,21,23,24,26,28–33] However, comprehensive experimental data with high enough time resolution and calculations mapping all the simultaneously populated decay paths are still lacking for this class of compounds, preventing a detailed picture of the ultrafast triplet state formation mechanisms.

Here, we combine broadband TA spectroscopy with sub-20 fs pulses in the UV and target analysis thereof with quantum mechanics/molecular mechanics (QM/MM) simulations to decipher the relaxation pathways of thio-substituted uracils in solution and model the TA experimental spectra (see Experimental Section and Supporting Information for details). We measure accurate singlet-state lifetimes leading to the triplet manifold of 2TU and 24TU, originating from simultaneously populated ππ* decay pathways, resolved by a detailed QM/MM computational mapping. This work establishes a unified view of the photophysics of thiouracils.

[a] D. C. Teles-Ferreira,[+] Dr. A. M. de Paula
Departamento de Física, Universidade Federal de Minas Gerais
31270-901 Belo Horizonte, MG (Brazil)
E-mail: ana@fisica.ufmg.br

[b] D. C. Teles-Ferreira[+]
Electrical Engineering Department, Federal Institute of Minas Gerais
Formiga, MG (Brazil)

[c] Dr. I. Conti,[+] Dr. A. Nenov,[+] Prof. M. Garavelli
Dipartimento di Chimica Industriale, Università degli Studi di Bologna
Viale del Risorgimento 4, 40136 Bologna (Italy)
E-mail: marco.garavelli@unibo.it

[d] Dr. R. Borrego-Varillas,[+] Dr. L. Ganzer, Dr. C. Manzoni, Prof. G. Cerullo
IFN-CNR, Department of Physics, Politecnico di Milano
P.za L. da Vinci 32, 20133 Milano (Italy)
E-mail: giulio.cerullo@polimi.it

[e] Dr. I. H. M. Van Stokkum
Department of Physics and Astronomy
Faculty of Sciences, Vrije Universiteit Amsterdam
De Boelelaan 1081, 1081HV Amsterdam (The Netherlands)

[+] These authors contributed equally to this work.

Supporting information and the ORCID identification number(s) for the author(s) of this article can be found under: https://doi.org/10.1002/chem.201904541.

## Results and Discussion

Figure 1 shows the chemical structures of the three investigated thiobases and the corresponding linear absorption (LA) spectra (dashed lines). The calculated spectra (solid lines)[3] are in satisfactory agreement with the experimental ones. Spectral decomposition (grey lines) of the computed LA spectra reveals a complex electronic structure consisting of two [ππ*(S2), ππ*′(S2)] and four [ππ*(S4), ππ*(S2), ππ*′(S4), ππ*′(S2)] bright components for 2TU and 24TU, respectively. Overlapping bands excited simultaneously by a specific pump pulse (red dashed lines) give rise to competing decay channels. Differently from previous studies,[3,23,24,27,34] which considered only the lowest ππ* state, we perform a complete analysis by mapping all decay pathways from the ππ* states populated simultaneously at a specific pump wavelength (ππ* grey overlapping bands in Figure 1) for the first time.

Figure 2 compares the TA spectra of the thiobases for different time delays. For 2TU (panel a) we observe the formation of two photoinduced absorption (PA, $\Delta A > 0$) bands: one in the UV (350–450 nm) and another in the visible (400–650 nm) range. Between these two bands in the 450–550 nm range there is at early delays a dip in the signal that we assign to a superposition of the PA with a stimulated emission (SE, $\Delta A < 0$) signal, as confirmed by the target analysis and calculations discussed later. For 24TU (panels b and c) we observe, for both 330 and 270 nm excitation wavelengths, a negative band at 360 nm assigned to the ground-state bleaching (GSB), because it corresponds to the ππ*(S4) peak in the LA spectrum (Figure 1, central panel). We also observe a broad, redshifted

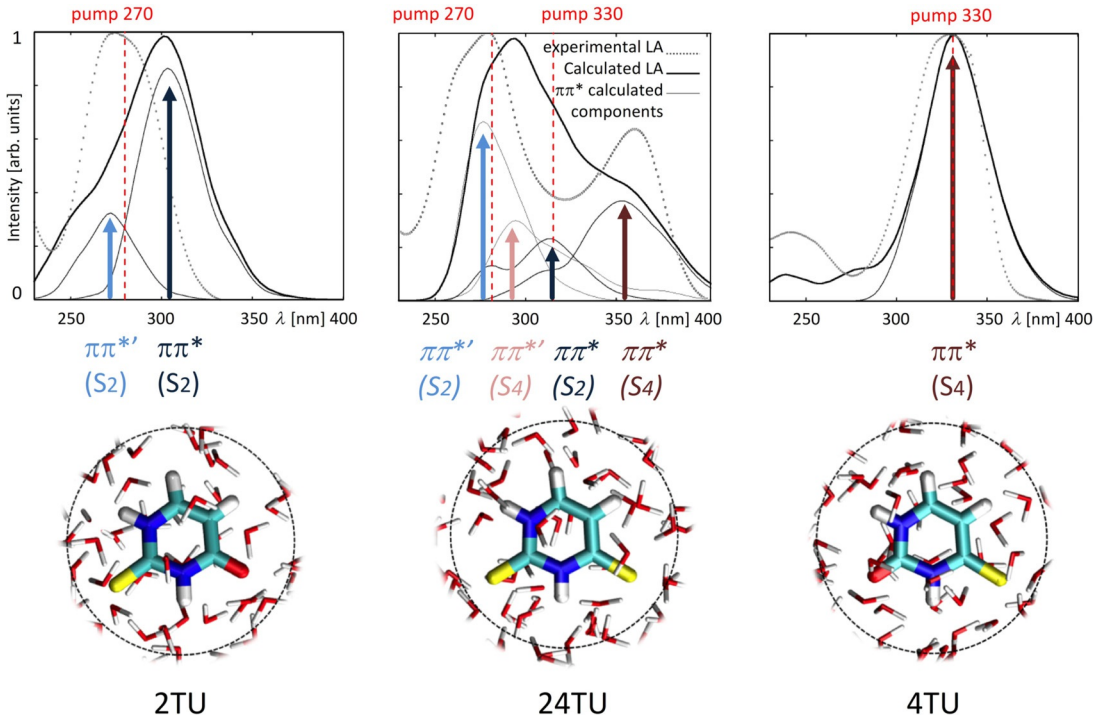


**Figure 1.** Experimental (dashed lines) and computed (black lines) LA spectra for 2TU and 4TU (at the MS-RASPT2/SA-6-RASSCF(12,9|2,4)/ANO-LS level) and for 24TU (at the MS-RASPT2/SA-9-RASSCF(2,2|14,10|2,2)/ANO-LS level), from Ref. [3]. Individual components, associated to specific ππ* electronic transitions, are shown in gray and their band maxima are indicated with arrows. State labels (Sx) are chosen according to the sulfur atom on which the frontier occupied orbitals are localized. The involved orbitals are documented in Figure S2 and Tables S1 and S2 (Supporting Information). Red dashed lines indicate the wavelength at which each system is excited in the TA experiments.

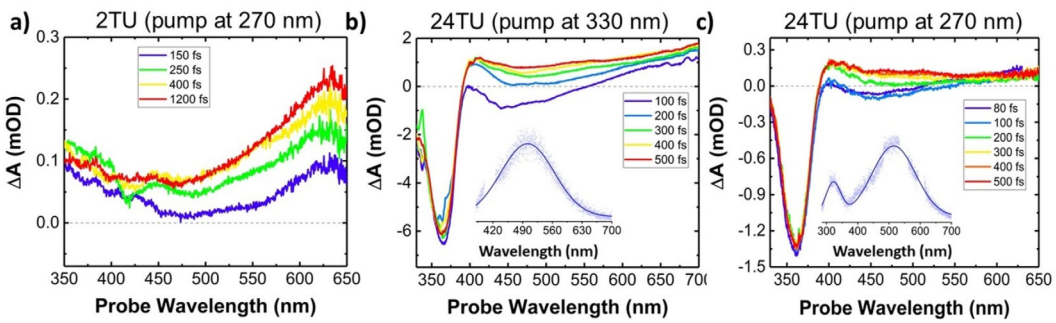


**Figure 2.** TA spectra at selected time delays: a) 2TU pumped at 270 nm. b) 24TU pumped at 330 nm. Inset: PL spectrum under excitation at 330 nm. c) 24TU pumped at 270 nm. Inset: PL spectrum under excitation at 270 nm.

negative band extending from 400 to 550 nm, which is assigned to SE. After about 200 fs the SE band evolves into a PA band which covers the 400–700 nm range. 2TU and 24TU dynamics at selected time delays are shown as insets in Figure 3 and Figure 4, respectively. Our previous studies on 4TU presents similar results, showing a SE band followed by the delayed build-up of a PA band in the visible.[29] The 24TU steady-state photoluminescence (PL) shows a broad peak in the visible (400–700 nm) for both excitation wavelengths (insets Figure 2). For the 270 nm pump there is also a small peak centered at 350 nm.

The TA data were subjected to target analysis, extracting the evolution-associated difference spectra (EADS) which, combined with the QM/MM calculations, allow to obtain an overall picture of the decay pathways. Figure 3 illustrates the decay pathways of 2TU excited at 270 nm. The EADS reveal an excited state that decays with a time constant of 167 fs (red line) into a long-lived product (blue line). There is no decay on the ground state within the time window of 2 ps and the fittings indicate a long-lived state $>1$ ns. The 167 fs EADS is characterized by a broad negative contribution, due to SE, between 400 and 650 nm and a narrow PA band peaking around 350 nm. The product does not show SE bands, but rather two distinct PA bands around 350 and 640 nm. We attribute the 167 fs EADS to the initially excited bright states $\pi\pi^*$(S2) and $\pi\pi^{*\prime}$(S2), whereas the product arises from the triplet manifold. QM/MM calculations allow to assign the observed spectral features and shed light on the underlying non-adiabatic processes. The photoexcitation at 270 nm (Figure 1) populates simultaneously two bright states—$\pi\pi^*$(S2) and $\pi\pi^{*\prime}$(S2)—each of which undergoes a different decay path, illustrated on the right and left hand side of Figure 3 (dark-blue and light-blue circles). The $\pi\pi^*$(S2) state relaxes in a local minimum [Min $\pi\pi^*$(S2)]. The 456 nm wavelength of the calculated vertical emission from Min $\pi\pi^*$(S2) is in good agreement with the peak of the negative contribution to the 167 fs EADS between 400–500 nm (highlighted in a full red box). The minimum is nearly isoenergetic with the minima on the $n\pi^*$ and $^3n\pi^*$ states, denoted Min $n\pi^*$(S2) and Min $^3n\pi^*$(S2). Moreover, the geometries of the three structures are nearly identical (see Figure S3, Supporting Information), suggesting the existence of a three-state near-degeneracy region allowing for the continuous exchange of population between them. Notably, according to our calculations, all three states contribute to an intense PA around 350 nm in the 167 fs EADS (highlighted as a hollow red box). We correlate this continuous population exchange to an increase of the $\pi\pi^*$ lifetime in 2TU, as compared to 4TU (results in Ref. [29]), for which we have recently reported a sub-100 fs lifetime, associated with the ballistic depopulation of the $\pi\pi^*$ state.[29] For the product EADS, the PA bands around 350 nm and between 550–700 nm (highlighted as hollow blue boxes) are in very good agreement with the calculated PAs of the lowest $^3\pi\pi^*$ triplet states [Min $^3\pi\pi^*$(S2) and Min $^3\pi\pi^{*\prime}$(S2)]. Similar bands have also been related to the triplet state in the literature.[21] The non-adiabatic decay pathway following excitation of $\pi\pi^{*\prime}$(S2) (left hand side of Figure 3) evolves through critical

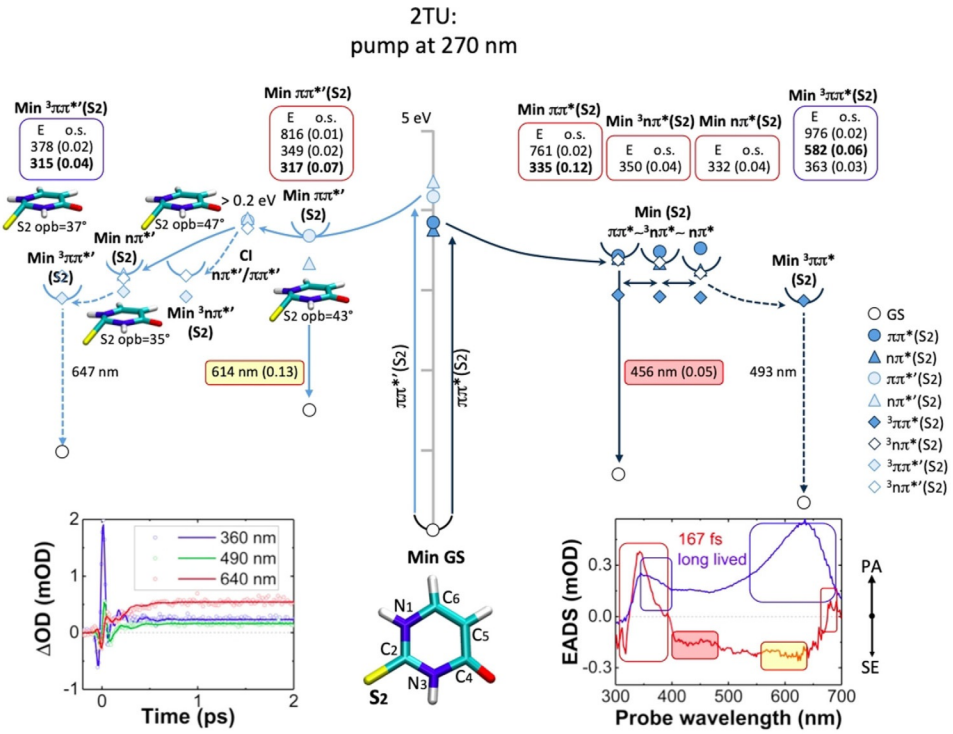


**Figure 3.** $\pi\pi^*$(S2) (on the right) and $\pi\pi^{*\prime}$(S2) (on the left) decay paths of 2TU, starting from the Franck–Condon region. The two bright states are excited with the same pump pulse at 270 nm. The insets shows the dynamics at selected wavelengths and the EADS with the corresponding time constants: 167 fs (red curve) and a long-lived product (blue curve). The calculated SE or PA energies and oscillator strengths (o.s.) are indicated in a red or blue box when they match with 167 fs or the product signals, respectively. For the calculated SE signals, the box background colors refer to different wavelength windows of the experimental ultrafast component (red curve, negative EADS signals).

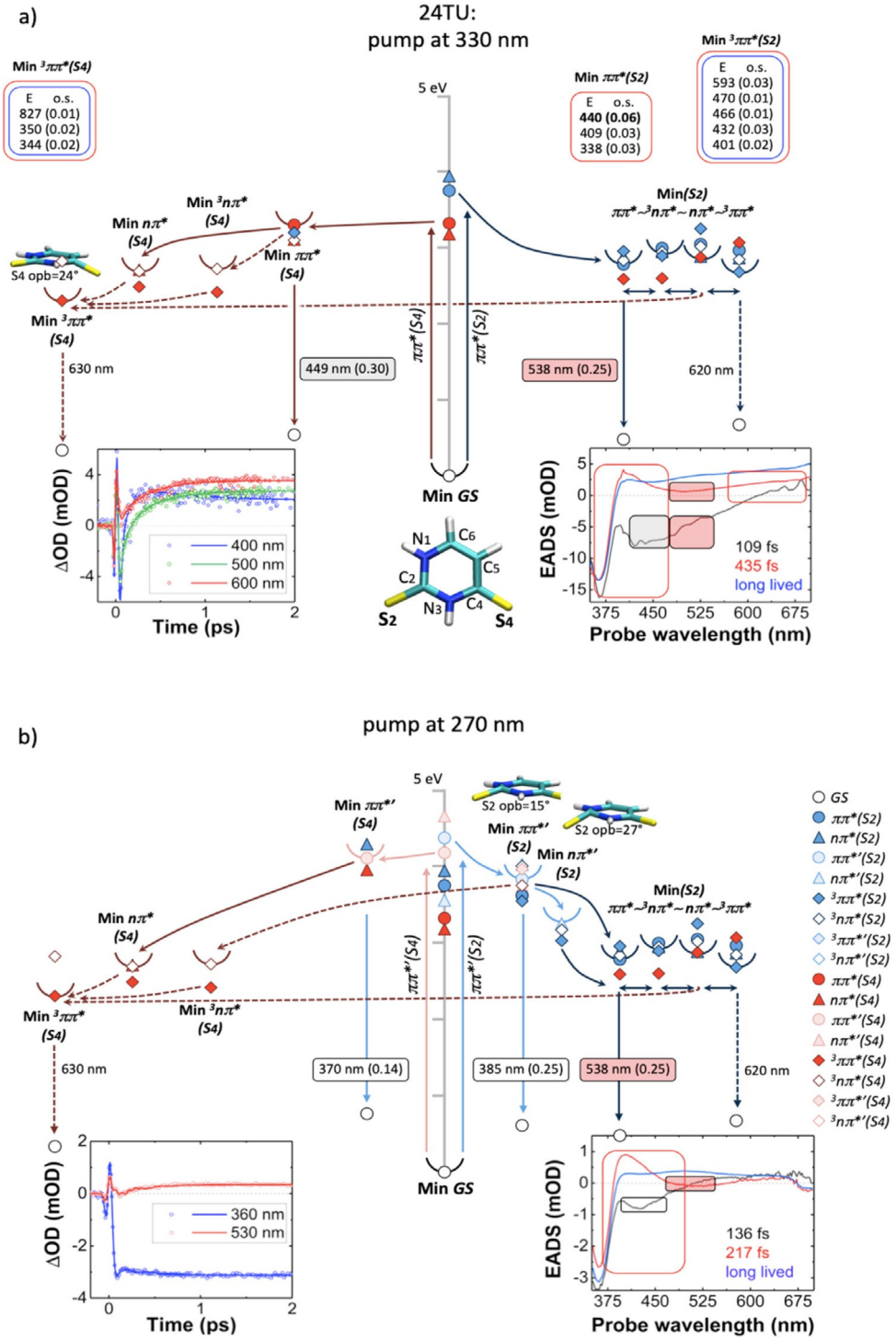


**Figure 4.** a) ππ*(S2) (on the right) and ππ*(S4) (on the left) decay paths, starting from the Franck–Condon region at 330 nm excitation wavelength. Insets: dynamics at selected wavelengths and EADS. b) ππ*′(S2) (on the right) and ππ*′(S4) (on the left) decay paths, starting from the Franck-Condon region at 270 nm excitation wavelength. Insets: dynamics at selected wavelengths and EADS. SE or PA values evaluated on all the minima are indicated with black, red and blue boxes according to the experimental lifetimes that they match. For the calculated SE signals, the box background colors refer to different wavelength windows of the experimental ultrafast component (black curve, negative EADS signals).

points decreasing in energy [Min ππ*′→Min $^3$nπ*′ or Min nπ*′→Min $^3$ππ*′(S2)]. However, a small barrier along the route to reach the ππ*′/nπ*′/$^3$nπ*′ degeneracy region (CI nπ*′/ππ*′) could increase the ππ*′ lifetime to a few hundred fs. Notably, this pathway exhibits a strong sulfur out-of-plane bending (contributing to the longer lifetime) in all involved electronic states, unlike the ππ*(S2) relaxation route described above, for which the system remains planar. This is attributed to the nodal structure of the π*′ orbital (Figure S2 and Table S1, Supporting Information) which leads to an increased

antibonding character. According to our calculations the Min ππ*′(S2) contribute to the intense PA at approximately 350 nm in the 167 fs EADS, as the Min ππ*(S2) region. The SE signal at about 600 nm in the EADS (highlighted in yellow) is typical of the ππ*′(S2) state, considering that it peaks at a similar wavelength to that of the calculated vertical emission from Min ππ*′(S2) (614 nm). Finally, the PA signal at about 350 nm in the product EADS (highlighted in a hollow blue box), corresponds to a transition from the Min $^3$ππ*′.

Summarizing, the observation of a broad 2TU SE band peaking in the range 400–500 nm and around 600 nm [matching with ππ* and ππ*′(S2) SE calculated energies, respectively; see Figure 3] strongly supports the hypothesis that the 167 fs lifetime could be addressed to the simultaneous population of both ππ*(S2) and ππ*′(S2), driving to the final long-lived triplet states.

Figure 4 shows the decay pathways of 24TU excited at 330 nm (upper panel) and 270 nm (lower panel). A target analysis of the 330 nm pump data (EADS in Figure 4a) reveals two time constants −109 fs (black) and 435 fs (red)—plus a long-living signal (blue). The 109 fs EADS shows a broad negative contribution (due to SE) peaking around 450 nm. The 435 fs EADS shows a broad positive signal (PA) covering the whole spectral window, which is superimposed with an SE band peaking around 500 nm, leading to a dip in the positive signal. The product shows a broad positive signal increasing in intensity for longer wavelengths. All EADS exhibit a strong narrowband negative signal around 360 nm, attributed to GSB. We assign the EADS to the initially excited bright states in the Franck–Condon region (109 fs) and after relaxation to the minimum (435 fs), whereas the product EADS arises from the triplet manifold trapping the population on a ns-timescale.

As can be seen in the computed LA spectra (Figure 1), two bright states—ππ*(S2) and ππ*(S4), denoted by dark blue and red circles in Figure 4a—are populated simultaneously by pumping at 330 nm. Each of them undergoes a different decay path, as indicated on the right- and left-hand side of Figure 4a. The ππ*(S2) state (right-hand side of Figure 4a) shows great similarities with the decay mechanism in 2TU. Upon relaxing to the local minimum, Min ππ*(S2), the calculated vertical emission of which (538 nm) matches with the tail of the negative signal above 475 nm in the 109 fs EADS, as well as with dip in the positive signal in the 435 fs EADS (highlighted in full red boxes), the population can undergo a non-adiabatic transfer to any of the states nπ*(S2), $^3$nπ*(S2) or $^3$ππ*(S2). Their corresponding minima show pronounced structural (see Figure S5, Supporting Information) and energetic resemblance, suggesting the continuous exchange of population between all four states, as also hypothesized for 2TU. The presence of a SE signature in the 435-fs EADS is indicative of the long ππ*(S2) lifetime. This is further corroborated by the calculations evidencing that the PA signal around 400–450 nm in the 435 fs EADS can only be attributed to the Min ππ*(S2) (highlighted in hollow red box). Notably, the 435 fs EADS resembles the product EADS at longer wavelengths (>550 nm), in support of the partial population of the lowest triplet state $^3$ππ* on the hundred-fs timescale.

We now turn our attention to the non-adiabatic decay path involving the ππ*(S4) state (left side of Figure 4a). The contribution to the negative signal at lower wavelengths (425–475 nm) in the 109 fs EADS (highlighted in a full grey box) is assigned to the SE from ππ*(S4). The analysis of the critical points reveals a barrierless path [Min ππ*→Min $^3$nπ* or Min nπ*→Min $^3$ππ*(S4)] connecting energetically well-separated minima, which do not exhibit significant out-of-plane distortions. This energy profile suggests the ballistic depopulation of the bright state, in agreement with the obtained 109 fs time constant. The hypothesis of the ultrafast depopulation of the ππ*(S4) state is supported by the absence of negative signal around 450 nm in the 435 fs EADS. Thus, rather than a relaxation process in the bright state, the two time constants 109 and 435 fs describe the parallel decay of the two ππ* states ππ*(S4) and ππ*(S2), respectively. We note the obvious similarities with the decay mechanism of the ππ*(S4) state in 4TU, for which we have recently reported an even shorter lifetime of 76 fs associated with a fast ππ*→nπ* decay in planar ring geometry.[29] Pumping at 270 nm, two other bright ππ* states, ππ*′(S2) and ππ*′(S4), denoted by light-blue and red circles—are populated, the decay paths of which are shown on the right- and left-hand side of Figure 4b. Target analysis reveals again two time constants −136 fs (black) and 217 fs (red)—plus a long-lived product state (blue). Overall, the EADS resemble their counterparts obtained from the 330 nm pump data target analysis, the main difference being the absence of the tail in the negative signal in the 136 fs EADS, now narrowed between 400–475 nm (highlighted in black box). Furthermore, we note the decrease of the intensity of the strong negative band at 360 nm between the 136 fs and 217 fs EADS. The spectral dynamics can be understood as the SE decay on a 136 fs timescale. Calculations show that the SE could be attributed to both ππ*′(S2) and ππ*′(S4), for which the vertical transition energies from their corresponding Min ππ*′(S2) and Min ππ*′(S4) fall at 370 and 385 nm, respectively. The calculated peak positions match the weak band in the PL spectrum (Figure 2c) visible only after 270 nm pump.

The resemblance between the 217 fs and the 435 fs EADS lifetimes, observed upon excitation at 270 or 330 nm, respectively, as well as between the long-lived EADS, suggests that, after departure from the initially populated ππ*′(S2) and ππ*′(S4) states, the system follows dynamics similar to the one observed after 330 nm pump, in agreement with Kasha's rule. This conclusion is reinforced by the PL spectra (Figure 2b,c) showing, for both pump wavelengths, a broadband peak at approximately 500 nm.

The joint analysis of the thio-substituted uracil derivatives 2TU, 24TU and 4TU[29] evidences that, although the decay paths activated through excitation of the bright ππ*/ππ*′ states are characterized by different energetics, lifetimes, and molecular distortions, they exhibit a common pattern. The ππ*/ππ*′ states relax either to their corresponding singlet nπ*/nπ*′ states or directly to the triplet manifold ($^3$nπ*/$^3$nπ*′) through an efficient ISC process. Eventually, the population is trapped in the lowest triplet state in each channel ($^3$ππ*/$^3$ππ*′). Our calculations strongly suggest the involvement of the dark

nπ*/nπ*′ states in the non-adiabatic decay, in agreement with a previous dynamical calculation[24] and time-resolved photoelectron spectroscopy experiments in the gas phase.[26,28,29,32] Nonetheless, the fingerprint PA signals of the nπ*/nπ*′ states are either weak in intensity (e.g., 24TU; for more details see Figures S6 and S7 in the Supporting Information) or coincide with more intense PA signals coming from the ππ*/ππ*′ states and the triplet manifold (e.g., 2TU; Figure S4, Supporting Information).

A deeper analysis of the ππ* decay pathways of the doubly substituted 24TU shows that they resemble the behavior observed for the single substituted 2TU or 4TU systems. This can be rationalized by looking at the shape of π orbitals. The ππ*(S2) transitions in 2TU and 24TU are defined by the same pair of π/π* orbitals, with the bonding orbital localized on $S_2$ (Figure 5a). Accordingly, we predict a similar deactivation mechanism characterized by population exchange between near-degenerate singlet/triplet states resulting in a comparably long ππ* lifetime. The ππ*(S4) transitions in 4TU and 24TU involve the same pair of π/π* orbitals with the bonding orbital localized on S4, leading to a similar ballistic decay route with a 100 fs ππ* time constant (Figure 5b). The ππ*(S4) decay path for 4TU is reported in Ref. [29]. Finally, the ππ*′(S2) transitions on 2TU and 24TU show an evident out-of-plane distortion of the $C_2$═$S_2$ group along the decay path, attributed to the nodal structure of the π*′ orbital, showing a nodal plane along the $C_2$═$S_2$ bond (Figure 5c), which facilitates out-of-plane deformations. The ππ*′(S4) decay path is not reported because at the excitation wavelength employed for 4TU (330 nm), this higher state is not populated due both to its blue shift and to its small intensity [see the 4TU ππ*′(S4) light-blue band in Figure S2, Supporting Information].

## Conclusions

In summary, we have presented a complete study of the simultaneous decay paths for solvated thiouracils, considering all the bright states showing overlapping ππ* linear absorption bands and disentangling the different paths giving rise to the dynamical features in the TA spectra. Comparing the three systems 2TU, 24TU and 4TU, we identify common features. 1) The photoexcited ππ* manifold features an ultrafast decay to the triplet manifold, where it remains trapped on the nanosecond timescale. This non-adiabatic decay happens either directly through an ISC process between the bright ππ* and the $^3$nπ* triplet states, or through an intermediate nπ* state, which remains spectroscopically elusive. 2) The former process leads to triplet formation on an approximately 100 fs timescale [167 fs for 2TU, 109/136 fs for 24TU and 76 fs for 4TU]. 3) Finally, the energetics and molecular deformations along the individual decay routes are correlated to the sulfur atom involved in the frontier π-orbitals, that is, $S_2$ or $S_4$, justifying the similarity of the behavior of 24TU with 2TU/4TU.

## Experimental Section

Femtosecond TA measurements used sub-20 fs pump pulses centered at 330 nm or 270 nm[35–37] and broadband probe pulses obtained by white-light generation in $CaF_2$, covering the 350–630 nm range. The instrumental response function was 25–35 fs FWHM,

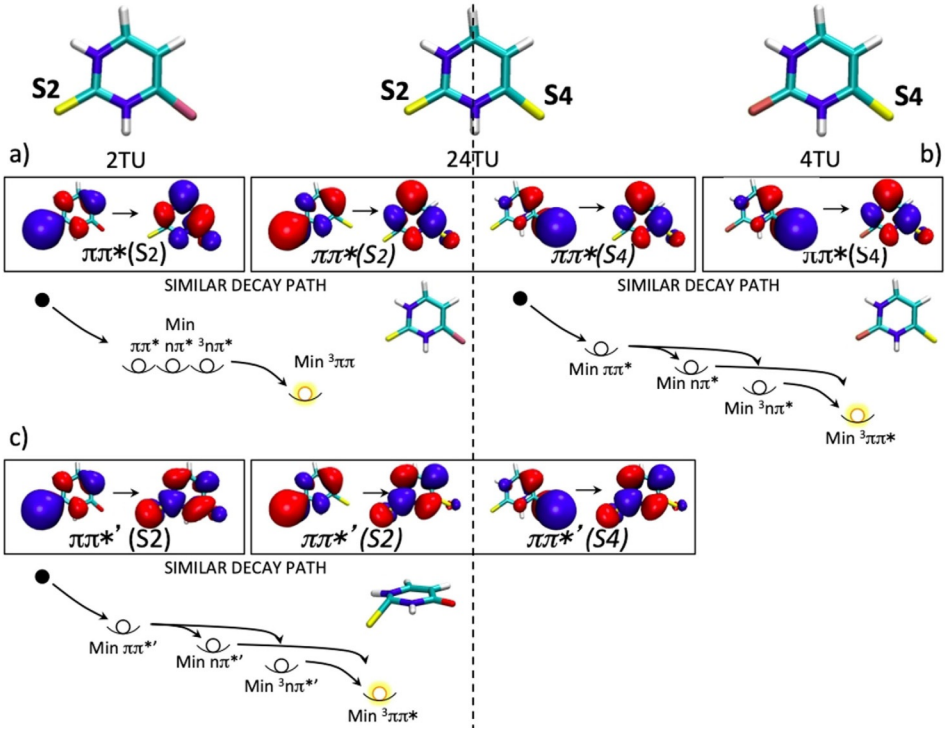


**Figure 5.** Molecular orbitals and schemes of the decay pathways for a) the ππ*(S2) and ππ*(S2) transitions on 2TU and 24TU; b) the ππ*(S4) and the ππ*(S4) transitions on 4TU and 24TU; c) the ππ*′(S2) and the ππ*′(S2) transitions on 2TU and 24TU.

depending on the probe wavelength. Samples were dissolved in phosphate buffer solution. Details on sample preparation and the experimental setup can be found in the Supporting Information. 24TU samples were pumped at 330 and 270 nm, whereas 2TU was pumped at 270 nm (see Figure 1). To describe the spectral evolution, we used global and target analyses with a sequential kinetic model.[38–40] We also measured steady-state photoluminescence (PL) at the same pump wavelengths.

### Computational Methods

The TA spectra and the decay paths were modeled by COBRAMM, our hybrid QM/MM scheme,[29,41–47] that couples high level ab initio multireference dynamically correlated methods (CASPT2//CASSCF)[48] of the photoactive thiouracil system with an explicit classical atomistic model (Amber force field)[49,50] of the solvent (see Supporting Information for more details).

An High/Medium/Low layers partitioning was applied to a spherical droplet centered at 2TU and 24TU with a radius of 12 Å (containing 261 and 265 waters), obtained from the cubic box. The QM region comprises the thionucleobase and the water molecules in 3 Å distance were included in the movable (MM) Medium layer (Figure S1, Supporting Information). The remaining water molecules were kept fixed in the (MM) Low layer. Ground-state geometry minimum was obtained using the optimizer of Gaussian 09[51] at the Møller–Plesset second-order perturbation theory (MP2) level as implemented in the Molcas 8 package[48] through its interface with COBRAMM. The excited-state geometry optimizations were computed at the MS-CASPT2 level (as implemented in Molcas 8 through its interface with COBRAMM), by using an active space including the sulfur lone pairs and the valence $\pi$-orbitals to a total of 12 electrons in 9 orbitals for 2TU and 14 electrons in 10 orbitals for 24TU (Tables S1 and S2, Supporting Information). The ANO-L basis set was used,[52] adopting contractions 5s4p2d1f on sulfur, 4s3p2d1f on carbon/oxygen/nitrogen and 3s2p1d on hydrogen atoms. The optimizing procedure is still done with the G09 optimizer, following the COBRAMM structure.

Critical points and conical intersections vertical energies were refined through a larger active space, extended by two bonding (n on O2 n and $\pi$ on sulfur) and one anti-bonding orbital ($\pi^*$ on sulfur, Table S1 and S2), together with an enlarged ANO-RCC basis set, adopting the contractions 6s5p3d2f1g on sulfur, 5s4p3d2f1g on carbon/oxygen/nitrogen and 4s3p2d1f on hydrogen atoms. So, an active space of (16e,12°) for 2TU and (18e,14°) for 24TU. Eleven states average calculations were employed.

The CASPT2 computations were always performed both in the single-state and multi-state approach. The ionization-potential-electron-affinity (IPEA) shift[53,54] was set to 0.0 and an imaginary shift[55] of 0.2 a.u. was used throughout. Transition dipole moments (TDMs) were calculated both at the SA-CASSCF level and at the MS-CASPT2 level by using the RASSI routine[56] of the Molcas code.

Conical intersections optimizations were performed with the gradient projection algorithm by Bearpark et al.,[57,58] as implemented in COBRAMM.[41]

## *Acknowledgements*

D.C.T.F. and A.M.d.P. acknowledge financial support from the funding agencies Fapemig, CNPq, and CAPES and INCT in Carbon Nanomaterials. We thank Dr. S. Santabarbara for preparing the PBS and T. A. S. Brandão (UFMG, Department of Chemistry) for helping with PL measurements. I.H.M.V.S. and G.C. acknowledge support from Horizon 2020 (Grant No. 654148, Laserlab-Europe). G.C. and M.G. acknowledge support from the H2020 Grant Agreement number 765266 (LightDyNAmics) and the European Research Council Advanced Grant STRATUS (ERC-2011-AdG No. 291198).

## Conflict of interest

The authors declare no conflict of interest.

**Keywords:** CASPT2 · conical intersections · QM/MM · thiobases · transient absorption · ultrafast spectroscopy

[1] B. Ashwood, M. Pollum, C. E. Crespo-Hernández, *Photochem. Photobiol.* **2019**, *95*, 33 – 58.
[2] S. Arslancan, L. Martínez-Fernández, I. Corral, *Molecules* **2017**, *22*, 998.
[3] A. Nenov, I. Conti, R. Borrego-Varillas, G. Cerullo, M. Garavelli, *Chem. Phys.* **2018**, *515*, 643 – 653.
[4] J. M. L. Pecourt, J. Peon, B. Kohler, *J. Am. Chem. Soc.* **2001**, *123*, 10370 – 10378.
[5] A. Nenov, J. Segarra-Martí, A. Giussani, I. Conti, I. Rivalta, E. Dumont, V. K. Jaiswal, S. F. Altavilla, S. Mukamel, M. Garavelli, *Faraday Discuss.* **2015**, *177*, 345 – 362.
[6] C. T. Middleton, K. de La Harpe, C. Su, Y. K. Law, C. E. Crespo-Hernández, B. Kohler, *Annu. Rev. Phys. Chem.* **2009**, *60*, 217 – 239.
[7] M. Pollum, S. Jockusch, C. E. Crespo-Hernández, *Phys. Chem. Chem. Phys.* **2015**, *17*, 27851 – 27861.
[8] B. Ashwood, S. Jockusch, C. E. Crespo-Hernández, *Molecules* **2017**, *22*, 379.
[9] M. Pollum, L. Martínez-Fernández, C. E. Crespo-Hernández, *Top. Curr. Chem.* **2014**, *355*, 245 – 327.
[10] M. Pollum, M. Lam, S. Jockusch, C. E. Crespo-Hernández, *ChemMedChem* **2018**, *13*, 1044 – 1050.
[11] C. Reichardt, C. E. Crespo-Hernaíndez, *J. Phys. Chem. Lett.* **2010**, *1*, 2239 – 2243.
[12] C. Reichardt, C. Guo, C. E. Crespo-Hernández, *J. Phys. Chem. B* **2011**, *115*, 3263 – 3270.
[13] O. Reelfs, P. Karran, A. R. Young, *Photochem. Photobiol. Sci.* **2012**, *11*, 148 – 154.
[14] A. Massey, Y. Z. Xu, P. Karran, *Curr. Biol.* **2001**, *11*, 1142 – 1146.
[15] A. Favre, G. Moreno, M. O. Blondel, J. Kliber, F. Vinzens, C. Salet, *Biochem. Biophys. Res. Commun.* **1986**, *141*, 847 – 854.
[16] M. Harris, H. Cote, C. Ochoa, C. Allavena, E. Negredo, P. Cahn, C. Zala, F. Raffi, *J. Acquired Immune Defic. Syndr.* **2009**, *50*, 339 – 340.
[17] K. M. Meisenheimer, T. H. Koch, *Crit. Rev. Biochem. Mol. Biol.* **1997**, *32*, 101 – 140.
[18] M. Pollum, S. Jockusch, C. E. Crespo-Hernández, *J. Am. Chem. Soc.* **2014**, *136*, 17930 – 17933.
[19] D. Valverde, A. Vasconcelos Sanches de Araujo, A. C. Borin, S. Canuto, *Phys. Chem. Chem. Phys.* **2017**, *19*, 29354 – 29363.
[20] X. Zou, X. Dai, K. Liu, H. Zhao, D. Song, H. Su, *J. Phys. Chem. B* **2014**, *118*, 5864 – 5872.
[21] M. Pollum, C. E. Crespo-Hernández, *J. Chem. Phys.* **2014**, *140*, 071101.
[22] See Ref. [20].
[23] S. Mai, P. Marquetand, L. González, *J. Phys. Chem. A* **2015**, *119*, 9524 – 9533.
[24] S. Mai, P. Marquetand, L. González, *J. Phys. Chem. Lett.* **2016**, *7*, 1978 – 1983.
[25] G. Cui, W. H. Fang, *J. Chem. Phys.* **2013**, *138*, 044315.
[26] S. Mai, A. Mohamadzade, P. Marquetand, L. González, *Molecules* **2018**, *23*, 2836.
[27] J. P. Gobbo, A. C. Borin, *Comput. Theor. Chem.* **2014**, *1040*, 195 – 201.
[28] A. Mohamadzade, S. Bai, M. Barbatti, S. Ullrich, *Chem. Phys.* **2018**, *515*, 572 – 579.

[29] R. Borrego-varillas, D. C. Teles-ferreira, A. Nenov, I. Conti, L. Ganzer, C. Manzoni, M. Garavelli, A. M. De Paula, G. Cerullo, *J. Am. Chem. Soc.* **2018**, *140*, 16087 – 16093.
[30] M. Ruckenbauer, S. Mai, P. Marquetand, L. González, *J. Chem. Phys.* **2016**, *144*, 074303.
[31] D. Koyama, M. J. Milner, A. J. Orr-Ewing, *J. Phys. Chem. B* **2017**, *121*, 9274 – 9280.
[32] J. A. Sánchez-Rodríguez, A. Mohamadzade, S. Mai, B. Ashwood, M. Pollum, P. Marquetand, L. González, C. E. Crespo-Hernández, S. Ullrich, *Phys. Chem. Chem. Phys.* **2017**, *19*, 19756 – 19766.
[33] J. Jiang, T. S. Zhang, J. D. Xue, X. Zheng, G. Cui, W. H. Fang, *J. Chem. Phys.* **2015**, *143*, 175103.
[34] L. Martinez-Fernandez, T. Fahleson, P. Norman, F. Santoro, S. Coriani, R. Improta, *Photochem. Photobiol. Sci.* **2017**, *16*, 1415 – 1423.
[35] A. Nenov, R. Borrego-Varillas, A. Oriana, L. Ganzer, F. Segatta, I. Conti, J. Segarra-Marti, J. Omachi, M. Dapor, S. Taioli, C. Manzoni, S. Mukamel, G. Cerullo, M. Garavelli, *J. Phys. Chem. Lett.* **2018**, *9*, 1534 – 1541.
[36] R. B. Varillas, A. Candeo, D. Viola, M. Garavelli, S. De Silvestri, G. Cerullo, C. Manzoni, S. De Silvestri, G. Cerullo, C. Manzoni, *Opt. Lett.* **2014**, *39*, 3849 – 3852.
[37] R. Borrego-Varillas, A. Oriana, F. Branchi, S. De Silvestri, G. Cerullo, C. Manzoni, *J. Opt. Soc. Am. B* **2015**, *32*, 1851 – 1855.
[38] J. J. Snellenburg, S. P. Laptenok, R. Seger, K. M. Mullen, I. H. M. van Stokkum, *J. Stat. Softw.* **2012**, *49*, 1 – 22.
[39] I. H. M. Van Stokkum, C. C. Jumper, J. J. Snellenburg, G. D. Scholes, R. Van Grondelle, P. Malý, *J. Chem. Phys.* **2016**, *145*, 174201.
[40] I. H. M. Van Stokkum, D. S. Larsen, R. Van Grondelle, *Biochim. Biophys. Acta Bioenerg.* **2004**, *1657*, 82 – 104.
[41] O. Weingart, A. Nenov, P. Altoè, I. Rivalta, J. Segarra-Martí, I. Dokukina, M. Garavelli, *J. Mol. Model.* **2018**, *24*, 271.
[42] I. Conti, L. Martínez-Fernández, L. Esposito, S. Hofinger, A. Nenov, M. Garavelli, R. Improta, *Chem. Eur. J.* **2017**, *23*, 15177 – 15188.
[43] I. Conti, P. Altoe, M. Stenta, M. Garavelli, G. Orlandi, *Phys. Chem. Chem. Phys.* **2010**, *12*, 5016 – 5023.
[44] A. Giussani, I. Conti, A. Nenov, M. Garavelli, *Faraday Discuss.* **2018**, *207*, 375 – 387.
[45] I. Conti, A. Nenov, S. Höfinger, S. F. Altavilla, I. Rivalta, E. Dumont, G. Orlandi, M. Garavelli, *Phys. Chem. Chem. Phys.* **2015**, *17*, 7291 – 7302.
[46] I. Conti, M. Garavelli, *J. Phys. Chem. Lett.* **2018**, *9*, 2373 – 2379.
[47] S. F. Altavilla, J. Segarra-Martí, A. Nenov, I. Conti, I. Rivalta, M. Garavelli, *Front. Chem.* **2015**, *3*, 29.
[48] F. Aquilante, J. Autschbach, R. K. Carlson, L. F. Chibotaru, M. G. Delcey, L. De Vico, I. F. Galván, N. Ferré, L. M. Frutos, L. Gagliardi, M. Garavelli, A. Giussani, C. E. Hoyer, G. L. Manni, H. Lischka, D. Ma, P. Å. Malmquist, T. Müller, A. Nenov, M. Olivucci, *J. Comput. Chem.* **2016**, *37*, 506 – 541.
[49] Amber 12, D. A. Case, T. A. Darden, T. E. Cheatham III, C. L. Simmerling, J. Wang, R. E. Duke, R. Luo, R. C. Walker, W. Zhang, K. M. Merz, B. Roberts, S. Hayik, A. Roitberg, G. Seabra, J. Swails, A. W. Götz, I. Kolossváry, K. F.Wong, F. Paesani, J. Vanicek, R. M.Wolf, J. Liu, X. Wu, S. R. Brozell, T. Steinbrecher, H. Gohlke, Q. Cai, X. Ye, J. Wang, M.-J. Hsieh, G. Cui, D. R. Roe, D. H. Mathews, M. G. Seetin, R. Salomon-Ferrer, C. Sagui, V. Babin, T. Luchko, S. Gusarov, A. Kovalenko, P. A. Kollman, University of California, San Francisco **2012**.
[50] R. Salomon-Ferrer, D. A. Case, R. C. Walker, *WIREs Comput. Mol. Sci.* **2013**, *3*, 198 – 210.
[51] Gaussian 09, Revision B01, M. J. Frisch, G. W. Trucks, H. B. Schlegel, G. E. Scuseria, M. A. Robb, J. R. Cheeseman, G. Scalmani, V. Barone, G. A. Petersson, H. Nakatsuji, X. Li, M. Caricato, A. Marenich, J. Bloino, B. G. Janesko, R. Gomperts, B. Mennucci, H. P. Hratchian, J. V. Ortiz, A. F. Izmaylov, J. L. Sonnenberg, D. Williams-Young, F. Ding, F. Lipparini, F. Egidi, J. Goings, B. Peng, A. Petrone, T. Henderson, D. Ranasinghe, V. G. Zakrzewski, J. Gao, N. Rega, G. Zheng, W. Liang, M. Hada, M. Ehara, K. Toyota, R. Fukuda, J. Hasegawa, M. Ishida, T. Nakajima, Y. Honda, O. Kitao, H. Nakai, T. Vreven, K. Throssell, J. A. Montgomery Jr., J. E. Peralta, F. Ogliaro, M. Bearpark, J. J. Heyd, E. Brothers, K. N. Kudin, V. N. Staroverov, T. Keith, R. Kobayashi, J. Normand, K. Raghavachari, A. Rendell, J. C. Burant, S. S. Iyengar, J. Tomasi, M. Cossi, J. M. Millam, M. Klene, C. Adamo, R. Cammi, J. W. Ochterski, R. L. Martin, K. Morokuma, O. Farkas, J. B. Foresman, D. J. Fox, Gaussian, Inc. Wallingford CT, **2010**..
[52] P.-O. Widmark, P. Å. Malmqvist, B. O. Roos, *Theor. Chem. Acc.* **1990**, *77*, 291 – 306.
[53] G. Ghigo, B. O. Roos, P. Å. Malmqvist, *Chem. Phys. Lett.* **2004**, *396*, 142 – 149.
[54] J. P. Zobel, J. J. Nogueira, L. González, *Chem. Sci.* **2017**, *8*, 1482 – 1499.
[55] N. Forsberg, P. Å. Malmqvist, *Chem. Phys. Lett.* **1997**, *274*, 196 – 204.
[56] P. Å. Malmqvist, *Int. J. Quantum Chem.* **1986**, *30*, 479 – 494.
[57] M. J. Bearpark, M. A. Robb, H. B. Schlegel, *Chem. Phys. Lett.* **1994**, *223*, 269 – 274.
[58] M. J. Bearpark, S. M. Larkin, T. Vreven, *J. Phys. Chem. A* **2008**, *112*, 7286 – 7295.

Manuscript received: October 3, 2019
Accepted manuscript online: November 21, 2019
Version of record online: December 10, 2019